JAERI-M
9589

HIGH DENSITY LOW-q DISCHARGES WITH D-SHAPED PLASMAS IN DOUBLET III

July 1981

Masayuki NAGAMI, Hidetoshi YOSHIDA, Kichiro SHINYA[*1]
G. JAHNS,[*2] Hideaki YOKOMIZO, Michiya SHIMADA
Kimihiro IOKI,[*3] Shigeru IZUMI[*4] and Masao KITSUNEZAKI

日本原子力研究所
Japan Atomic Energy Research Institute

この報告書は，日本原子力研究所がJAERI-Mレポートとして，不定期に刊行している研究報告書です．入手，複製などのお問合わせは，日本原子力研究所技術情報部（茨城県那珂郡東海村）あて，お申しこしください．

JAERI-M reports, issued irregularly, describe the results of research works carried out in JAERI. Inquiries about the availability of reports and their reproduction should be addressed to Division of Technical Information, Japan Atomic Energy Research Institute, Tokai-mura, Naka-gun, Ibaraki-ken, Japan.

JAERI-M 9589

High Density Low-q Discharges with D-Shaped Plasmas in Doublet III

Masayuki NAGAMI, Hidetoshi YOSHIDA, Kichiro SHINYA[*1]
G. JAHNS[*2], Hideaki YOKOMIZO, Michiya SHIMADA
Kimihiro IOKI[*3], Shigeru IZUMI[*4] and Masao KITSUNEZAKI

Division of Large Tokamak Development,
Tokai Research Establishment, JAERI

(Received July 8, 1981)

The maximum plasma current in Doublet III is found to be limited by disruptions when the limiter safety factor is approximately 2. However, due to the strong toroidal and shaping field effect on rotational transform at the outer plasma edge associated with a D-shape formation having a vertical elongation of 1.5, the safety factor q_a^* estimated from simple geometric considerations for D-shaped plasmas corresponds to values as low as 1.5. These discharges operate stably with considerably higher plasma current than most reactor design studies assume. These low-q discharges show excellent plasma performance: very flat spatial electron temperature profiles, high density operation with $\bar{n}_e R/B_T$ up to 7.8, and good energy confinement producing a volume average β of up to 1% with ohmic heating only. This operational regime appears to be applicable to future high β tokamaks with D-shaped cross section.

Keywords; Doublet-III, Low-q, D-shaped Cross Section, Plasma Current, β Value, Joule Heating

---

*1 On leave from Toshiba Corp.
*2 General Atomic Company, San Diego, California, U.S.A.
*3 On leave from Mitsubishi Atomic Power Industries
*4 On leave from Hitachi Ltd.

JAERI－M 9589

ダブレッドⅢにおけるD型断面プラズマの高密度低安全係数放電

日本原子力研究所東海研究所大型トカマク開発部

永見　正幸・吉田　英俊・新谷　吉郎[*1]
G. JAHNS[*2]・横溝　英明・嶋田　道也
伊尾木公裕[*3]・出海　　滋[*4]・狐崎　晶雄

（1981年7月8日受理）

ダブレッドⅢにおける安全係数の最小値は約2である。

しかしながら，D形断面プラズマでは，トロイダル効果と形状制御磁場により安全係数がプラズマ表面で急激に増大するため，単純に断面形状のみを考慮した安全係数では1.5まで安定な放電が得られる。これは従来の炉設計で想定しているプラズマ電流の値をはるかに上回る値である。低安全係数放電により以下に示す優れたプラズマ性能が得られる。1）高プラズマ密度（村上係数7.8）2）平担な温度分布，3）ジュール加熱のみで体積平均ベータ値1％。

＊1）外来研究員；東京芝浦電気㈱
＊2）General Atomic Company
＊3）外来研究員；三菱原子力工業㈱
＊4）外来研究員；日立製作所㈱

Contents

目　　次

1. INTRODUCTION

In most recent experiments in ISX-B [1], the values of $\langle\beta\rangle$ (volume averaged β) ~ 2.5% reported from ISX-B and JFT-2 [2] have not been exceeded even though the neutral beam power has been raised. In the β saturation study, β saturation appears in β_p (poloidal β) rather than β (toroidal β), i.e., the $\langle\beta\rangle$-values achievable in ISX-B show a clearly favorable trend with increasing plasma current as in $\langle\beta\rangle \propto \beta_p I_p^2/B_T^2 \propto \beta_p/q_a^2$. On this empirical basis, the smallest q-values consistent with disruption-free operation become quite an important requirement for achieving high β plasmas in future tokamak reactors. Generally, low-q discharges are believed to be disruptive. A low-q discharge of $q_a < 2$ was realized in TOSCA [3], T-11 [4], T-10 [5], Alcator-A [6]. However, in these experiments, reproducible freedom from major disruption was not observed. The very low-q discharge of $q_a < 2$ demonstrated in DIVA [7] shows a reliable non-disruptive regime; with a close conducting shell and titanium gettering, experiments in DIVA have demonstrated that a major disruption cannot be excited in a $q_a < 2$ discharge. Thus, very low-q operation is considered to be an important approach in eliminating the possibility of causing a dangerous major disruption resulting in large electromagnetic and thermal loads on the plasma chamber wall.

This paper reports the experiments performed in Doublet III in order to explore reliable low-q operational regimes for future high β tokamaks with D-shaped cross sections and without a conducting shell.

In our experiment, stable discharges with $q_a < 2$ were not realized. However, a new operation regime, which is expected to improve the high β capability of tokamaks, was found. Due to the strong effect of the toroidal and shaping field on rotational transform at the plasma periphery associated with the D-shape formation, the q values of D-shaped plasma increase sharply at the plasma outer edge. The resultant q-value at the energy confinement region is very small; e.g., $q < 1.5$ at $r/a < 0.86$-0.9 for $q_a = 2.9 - 2.5$, where the discharges have reproducible stability.

As a result, low-q discharges with D-shaped cross sections, showed excellent plasma performance: 1) a high plasma current operational capability (a factor of 2 higher than those of circular plasmas) with good MHD stability, 2) very flat electron temperature and plasma current profiles in the plasma cross section, 3) a high density operation capability of $\bar{n}_e R/B_T$ [$\times 10^{19}$ m^{-2} T^{-1}] up to 7.8, and 4) good energy confinement producing a volume average beta reaching 1% with ohmic heating only.

Section 2 discusses the experimental arrangement; Section 3, MHD equilibria; Section 4, formation and stability of low-q discharges; Section 5, energy confinement; Section 6, plasma-wall interaction. The conclusions are discussed in Section 7.

2. EXPERIMENTAL ARRANGEMENT

Figure 1 shows a cross section view of Doublet III. The Doublet III tokamak [8] has the following parameters: major radius R ≅ 141 cm, plasma width 2a ≅ 88 cm. The Inconel 625 vacuum vessel is surrounded by 24 field-shaping coils. Feedback control of the magnetic flux linking the shaping coils allows the shape and position of many types of discharge to be controlled very precisely [9]. Arbitrary waveforms can be specified for the plasma current waveform and gas puffing system throughput by using waveform generators. These parameters are feedback controlled.

In these low-q experiments, TiC coated POCO-graphite plates with water cooling are used as a primary limiter (Fig. 1). The graphite limiter was installed in the summer of 1980 in place of the Inconel limiter. The primary limiter is placed ~ 5 cm from the wall. On the inside and top of the wall, Inconel limiters positioned 3 cm from the wall are used (we call them back-up limiters). There are 8 inside back-up limiters and 3 top back-up limiters. Ti gettering which covers the wall with an average monolayer of 0.1-0.2 was employed during each sequence of shots.

The plasma diagnostics used for the present study are:

1. Plasma equilibrium: 24 single turn flux loops to measure the distribution of the poloidal flux values on the 24 shaping coils,

and 12 magnetic probes to measure the distribution of the poloidal magnetic field. The flux surface in the plasma cross section is calculated with an MHD equilibrium code [10].

2. Density distribution $n_e(r)$: 5-channel tangential CO_2 laser interferometers.

3. Electron temperature distribution $T_e(r)$: scanning soft X-ray energy spectrometer.

4. Radiative power loss: 5-channel and 21-channel bolometer arrays.

5. MHD activity: 12-channel tangential and 19-channel vertical soft X-ray diode arrays.

3. PLASMA EQUILIBRIA

The plasma current waveforms and MHD equilibria for the typical stable lowest q_a^* discharges of D-shaped and circular plasmas are shown in Fig. 2.

1. $K_a = 1.55$, $I_p = 760$ kA, $B_T = 10$ kG, $q_a^* = 1.54$, $\bar{n}_e = 5.0 \times 10^{13}$ cm^{-3}

2. $K_a = 1.12$, $I_p = 540$ kA, $B_T = 12$ kG, $q_a^* = 1.67$, $\bar{n}_e = 4.8 \times 10^{13}$ cm^{-3}

Here, q_a^* is defined as

$$q_a^* = \frac{2\pi a^2 B_T}{\mu_o I_p R_o} \cdot \frac{1 + K_a^2}{2} ,$$

where K_a, a, R_o are the vertical elongation at the outermost magnetic surface, plasma horizontal minor radius and major radius, respectively. These discharges are stable during ~ 300 msec flattop of the plasma current, and terminated by volt-second limitation. At t ~ 890 msec the plasma current decays very rapidly due to the termination of the power supply for plasma position control. Plasma equilibria at the flattop phase are analyzed by MHD equilibrium codes. The poloidal flux values measured at the 24 shaping coils are used as the boundary condition for the calculation. The plasma current profiles are chosen to have the best fit the calculated magnetic field to the measured magnetic field at the shaping coils.

Figure 3 shows the distribution of q^{ψ} as a function of the minor radius, where q^{ψ} is the MHD q determined as

$$q^{\psi} = \frac{R B_T}{2\pi} \int \frac{dl}{R^2 B_p} \quad .$$

Here the integration is made along the equilibrium poloidal field lines. For D-shaped and circular cross-section plasmas, q^{ψ} is smaller than 1 and stays at ~ 0.95 at the horizontal minor radius of $r < 29$ cm and 25 cm, and sharply increases at the plasma outer edge. The calculated radius of q = 1 magnetic surface shows reasonable agreement with the observation of sawtooth inversion by soft X-ray diode arrays. q^{ψ} at the plasma surface ($q_a{}^{\psi}$) attains 2.35 for D-shaped plasmas of $q_a{}^* = 1.54$, and 2.00 for circular plasmas of $q_a{}^* = 1.67$. Note that the discrepancy between $q_a{}^{\psi}$ and $q_a{}^*$ is large in the non-circular case: $q_a{}^{\psi}/q_a{}^* = 1.52$ for the D-shaped plasma, $q_a{}^{\psi}/q_a{}^* = 1.20$ for the circular plasma.

Although the outermost plasma surface of D-shaped plasmas are not a simple elliptic configuration, the real circumference ($\ell_p = \int dl$) is almost equal ($\ell_p/\ell_p' = 0.99$) to the elliptic assumption of $\ell_p' = 2\pi a\sqrt{(1 + K_a{}^2)/2}$. Therefore, the elliptic assumption of the magnetic surface in calculating $q_a{}^*$ cannot account for the difference between $q_a{}^*$ and $q_a{}^{\psi}$. Figure 3 shows that the difference between $q_a{}^{\psi}$ and $q_a{}^*$ is ascribed to the toroidal effect $R_0{}^2\langle R^{-2}\rangle$ (1.33 for D-shaped plasma, 1.22 for circular plasma) and the effect of the equilibrium magnetic field produced by field-shaping coil currents

$\langle B_p \rangle / \langle B_p' \rangle$ (1.14 for D-shaped plasma, 1.02 for circular plasma), both sharply increase at the plasma periphery, where

$$\langle B_p \rangle = \int B_p \, dl / \int dl, \qquad \langle B_p' \rangle = \int dl / \int B_p^{-1} \, dl$$
$$\langle R^{-2} \rangle = \int R^{-2} \, dl / \int dl \quad .$$

Figure 4(a) shows the observation of the magnetic surface of sawtooth inversion with 19-channel vertical and 12-channel tangential soft X-ray diode arrays for discharges with $q_a^* = 1.5$, 2.1, and 3.1. Figure 4(b) shows the vertical elongation of the $q = 1$ magnetic surface obtained by soft X-ray diode observation and that of the calculated outermost magnetic surface as a function of $1/q_a^*$.

For the same control of the magnetic flux surfaces linking at the field-shaping coils for each discharge, the elongation of the magnetic surface at the limiter position increases from 1.42 to 1.52 with the decrease of q_a^* from 3.1 to 1.5. At the same time, the vertical elongation of the $q = 1$ magnetic surface measured with soft X-ray diodes increases from 1.18 to 1.38. This is due to the flattening of the plasma current profile with the decrease of q_a^*; in the equilibrium analysis the best agreement with the experiment was obtained with ℓ_i (non-dimensional internal inductance) from 1.3 to 0.9 for the q_a^* from 3.1 to 1.5. In order to simply scale q_a^* with the magnitude of plasma current, we will employ $K_a = 1.47$ of $q_a^* = 2$ shown in Fig. 4(b) for D-shaped plasmas with arbitrary q_a^* in all the figures after Fig. 4. Figure 4(b) also shows that the toroidal and shaping field effect on rotational transform is almost constant for

arbitrary q_a^*. Therefore q_a^{ψ} scales linearly with q_a^*.

Figure 4(c) shows the ratio of the horizontal radius of the sawtooth inversion magnetic surface r_s to the horizontal minor radius as a function of q_a^{*-1}. With the decrease of q_a^*, $r_{s/a}$ increases in a similar manner up to ~ 0.5 for both D-shaped and circular plasmas.

4. FORMATION AND STABILITY OF LOW-q DISCHARGE

The important operational conditions for achieving stable low-q discharges are listed below. When the conditions discussed here do not exist, discharges usually have major disruptions during the current ramping phase.

1. Clean wall and limiter surface: good vacuum condition and a moderate amount of Ti gettering (~ average 0.1-0.2 monolayer/shot) is necessary. The base pressure of the chamber before starting the day's operation was $0.8 - 5 \times 10^{-8}$ Torr.

2. Selection of limiter material; when the Inconel plate with water cooling was used as the primary limiter (before the summer of 1980), repeated operations with more than 4 or 5 shots with a plasma current >700 kA were difficult even in B_T = 24 kG ($q_a^* \sim 3.0$) due to melting of the surface during discharge (drops of melted Inconel were observed by TV) which caused major disruptions of the plasma. After TiC coated POCO-graphite was installed as the primary limiter, repeated operations of 1 MA became possible.

3. Precise conditioning of plasma position: precise tuning of the radial (less than ±0.5-1 cm) and vertical (less than ±1.5-2 cm) position controls which are used to minimize heat load on any one particular area of the limiter is important. This is directly related to plasma-limiter interaction which results in a release

of dangerous amounts of limiter material.

4. Slow ramping of plasma current and adjustment of gas puff throughput during the ramping phase of the plasma current; It is very difficult to achieve a low-q discharge with a ramping rate faster than 1.5 MA/sec. Below this current ramping rate, there is a narrow window in adjusting gas puff throughput. This limits the region of (n_e, I_p) space at the flattop phase of stable low-q discharge.

A stable operational regime in an average electron density of $\bar{n}_e$ and I_p with B_T = 12 kG at the flattop phase of the discharge is shown in Fig. 5. This data was taken during 3 weeks of operations (7 days for this low-q experiment) when the vacuum was very well conditioned. After this series of experiments, a minor air leak through the primary limiter support occurred (the base pressure before the start of operations was 1 -3 x 10^{-7} Torr) which made it impossible to achieve a plasma current of more than 600 kA with 12 kG (q_a^* = 2.1) for D-shaped plasmas. The maximum operational I_p before the leak was 870 kA and 540 kA for stable D-shaped and circular cross section plasmas with B_T = 12 kG with each corresponding to a q_a^ψ of 2.4 and 2.0. The difference in the stable I_p operation capabilities of D-shaped and circular plasmas is larger than the ratio of q_a^*, i.e., $(1 + K_a^2)/2$. Under the assumption that the m/n = 2/1 tearing mode dominates the disruptive instability, as is clearly shown in DIVA, and that the stability of the mode is very sensitive to the slight change of current profile when the q^ψ = 2 surface is very close to the plasma surface [11], the large difference in stable I_p operation capability may be due to the strong toroidal and shaping field effect on the q_a^ψ for D-shaped plasmas, which move the q_a^ψ = 2 resonant

surface toward the center of the plasma for a given I_p.

For $q_a^* < 2$, circular plasmas show higher $\bar{n}_e$ operation capability than D-shaped plasmas with the same I_p. This was previously discussed in Ref. [12] for high-q plasmas as maximum operational $\bar{n}_e$ is determined by q_a^* for the same B_T, i.e., in order to obtain the same maximum plasma density achieved in circular plasmas, D-shaped plasmas need a larger plasma currents than circular plasmas corresponding to the identical q_a^* for the same B_T. In a low-q regime of $q_a^* < 2$, however, D-shaped plasmas can extend the operational regime of $\bar{n}_e$ much higher due to the large I_p operation capability.

Figure 6 shows the dependence of stability on gas puff throughput Q during the plasma current ramping phase: a) stable discharge of I_p = 750 kA with Q = 80 Torr l/sec, b) disruptive discharge with small Q of 60 Torr l/s, c) disruptive discharge with large Q of 93 Torr l/s. The dependence of stability on gas puff throughput was very reproducible. With a small Q, there is little radiative cooling at the outer edge of the plasma. This causes a high nickle impurity influx as shown in Ni XI intensity, and results in plasma disruption. In case c), large amounts of gas puffing causes strong cooling of the plasma edge. At the same time, a strong increase in nickel impurity influx was observed.

These results show that adjusting the intensity of the gas puff throughput during current ramping is an essential requirement in order to achieve low-q discharge. A similar phenomenon was observed in Ref. [11], in which it was explained that stability is determined by modification of the

plasma current profile near $q^{\psi} = 2$ magnetic surface with gas puffing. In the present experiment, gas puff control is also directly related to the control of metallic impurity production at the limiter. As a result, stable low-q discharges with a high plasma current of ~850 kA are controlled to have the same amount of nickel as low plasma currents of ~420 kA.

Once stable operation conditions, such as plasma current and gas puff waveform, and plasma positioning are established, low-q discharges, especially D-shaped plasmas, show good reproducible MHD stability.

Figure 7 shows the probability of disruption as a function of programmed I_p at the flattop for D-shaped plasmas with B_T = 12 kG. Here, we refer only to discharges produced after stable operation conditions were estabished. Conditioning discharges to find stable operation region and discharges with neon gas injection to test the stability are excluded.

For a programmed I_p of greater than 900 kA, the discharge always disrupts. For a programmed I_p of less than 900 kA, the number of shots referred to here are: total 165 shots, stable discharge 145 shots (88%), disrupted discharge 20 shots (12%) (during flattop 6 shots, during current ramp 14 shots). In discharges with $q_a^* < 2$, disruption occurs mainly during the I_p ramping phase. Note that the number of disruptions during the flattop is quite small.

Figure 8 shows the locations of disruption in the n_e-I_p space for all the disrupted shots (20 shots). Each location corresponds to the time when the first negative spike appeared in I_p. The trajectories of two

typical stable discharges are also shown: a lowest n_e and a highest n_e operation with I_p = 850 - 870 kA at the flattop. The figure shows that disruptions during the flattop (shown as X) occur at the very edge of the stable region of $\bar{n}_e$-I_p. One shot with the highest $\bar{n}_e$ with I_p = 870 kA is even outside the stable region. This disruption happed during an operation of repeated discharges achieving $\bar{n}_e$ and I_p at the very edge of the stable region with the same gas puff throughput, and is apparently due to change of surface conditions during repeated operations.

The disruptions during the current ramp phase (shown as symbol of ●) may be grouped into three types: 1) disruptions near the higher $\bar{n}_e$ stability boundary. These disruptions are caused by relatively large gas puff throughput in discharges aiming to achieve high $\bar{n}_e$ at the flattop phase; 2) disruption near the lower $\bar{n}_e$ stability boundary. These disruptions are caused by relatively small gas puffing in discharges aiming to achieve low $\bar{n}_e$ at the flattop. Two disruptions at I_p = 730 kA, $n_e = 3.2 \times 10^{13}$, 3.3×10^{13} cm^{-3} occurred after a longer break time during shots (~30 min) than usual (~7 min). The longer break time causes relatively small $\bar{n}_e$ due to the change in surface condition of the chamber wall; and 3) disruptions at the beginning (~100 ms) of the discharge.

This result suggests the possibility of large reduction in probability of disruption; disruption can be prevented if the n_e-I_p at the flattop is aimed well inside of the stability boundary and if the discharge trajectory is carefully selected to pass through the center of the stable region. Disruption at the initial phase may not be a serious problem in the future in terms of damage to the plasma chamber, because those discharges can be

artifically terminated before the I_p is ramped much higher.

Figure 8 also suggests that stable regions can be simplified using three lines; between two lines of I_p/n_e = 1.1 and 2.2 MA/10^{14} cm^{-3} and below the horizontal line corresponding to $q_a^{\Psi} \sim 2.4$ ($q_a^* \sim 1.5$).

For $I_p > 870$ kA, the discharge always disrupts with B_T = 12 kG. At B_T = 10 kG, however, a reproducible stable operation of I_p = 760 kA is possible, which corresponds 912 kA with B_T = 12 kG. From this evidence, the lowest stable q_a is considered to be determined not only simply by q_a^{Ψ}-value, but also by the ohmic input power and severity of plasma-wall interaction.

Figure 9 shows the stable operational regime in ($n_e R/B_T$, $1/q_a^*$) space. Typical low-q discharges shown in Fig. 5 are referred to here as well as discharges before the start of Ti gettering (March, 1980) and discharges before installation of the graphite primary limiter (August, 1980) [13]. The low-q discharge regime, especially of D-shaped plasmas, shows the high density operational capability reaching $\bar{n}_e/B_T/R$ = 7.8 ($\times 10^{19}$ m^{-2} T^{-1}) with ohmic heating only.

5. ENERGY CONFINEMENT

Typical electron temperature profiles for discharges of 12 kG, $K_a \sim 1.5$, $q_a^* = 1.5$ and 2.8 measured with a scanning soft X-ray spectrometer (1-10 keV) are shown in Fig. 10. With the decrease in q_a^*, the electron temperature profile becomes flat. In the low-q_a^* and high $\bar{n}_e$ operation shown here, the volume average β reaches 1.0% with ohmic heating only. The electron density profile measured with a 5-channel CO_2 laser interferometer is usually flat ($\bar{n}_e \sim 1-(r/a)^4$) for arbitrary q_a^*.

The scaling of the global electron energy confinement time $\tau_{E_{eG}}$ for discharges of $1.4 < q_a^* < 3.2$ in circular and 1.5 elongated D-shaped plasmas is shown in Fig. 11, where $\tau_{E_{eG}} = \int 3/2\ n_e\ T_e\ dV/I_p\ V_\ell$.

A least square fitting of the data assuming linear dependence of $\tau_{E_{eG}}$ on $\bar{n}_e$ yields global electron energy confinement time scales like

$$\tau_{E_{eG}}\ (\text{msec}) = 30\ \bar{n}_e\ [\times 10^{14}\ \text{cm}^{-3}]\ q_a^{*0.84} \quad .$$

The global energy confinement time τ_E (electrons and ions) is twice that of $\tau_{E_{eG}}$ because the ion heat transport calculation using up to 2 times neoclassical transport predicts that $T_e \simeq T_i$ in all the discharges in Fig. 11

(the ion temperature was not measured in this series). Then the present scaling in Doublet III can be written as

$$\text{D-III low-q:}\quad \tau_E[\text{sec}] = 0.3\ \bar{n}_{e_{14}}\ q_a{}^{*0.84}\ a^2 \quad ,$$

where $n_{e_{14}} = n_e/10^{14}$ cm^{-3} and a in meter. In comparison with INTOR scaling presently used for future reactor design,

$$\text{INTOR:}\ \tau_E[\text{sec}] = 0.5\ \bar{n}_{e_{14}}\ a^2$$

these confinement scalings show identical τ_E at $q_a{}^* = 1.8$. Therefore, the present low-q regime of $q_a{}^* \sim 1.8$ in Doublet III is fairly well applicable to future reactor design.

In these discharges, energy confinement is mainly determined by electron energy transport. Up to 2 times the neoclassical heat loss of ions and radiative power loss is not the major part of the energy loss.

Therefore, the electron energy confinement time τ_{Ee} is proportional to $\bar{n}_e\ q_a{}^{*0.84}$, and can be approximated as

$$\tau_{E_e} \propto \bar{n}_e\ q_a{}^* \propto \bar{n}_e\ \frac{B_T}{I_p}\ \frac{1 + K_a^2}{2} \quad .$$

This shows that for constant B_T and I_p, electron energy confinement improves by $(1 + K^2)/2$ with vertical elongation. For constant $q_a{}^*$, electron energy confinement time is the same for both circular and non-circular plasmas [12].

In the low-q discharges of DIVA [7], strong sawtooth oscillations are observed in the electron temperature and soft X-ray emissions from the plasma center. The energy confinement is strongly affected by internal disruption spreading to more than half the minor radius. The period of sawtooth oscillation t_s is proportional to n_e/q_a, and the amplitude $(\Delta (n_eT_e)/(n_eT_e)$ is roughly proportional to $q_a^{-3/2}$. This sawtooth oscillation results in an energy confinement time proportional to $n_e\, q_a^{1/2}$, since the energy confinement time determined by sawtooth oscillation $\tilde{\tau}_{E_e}$ is described as

$$\tilde{\tau}_{E_e} = n_eT_e/(\Delta(n_eT_e)/t_s) \quad . \tag{1}$$

In Doublet III, sawtooth oscillation is an important but not major cause of electron energy transport even though the internal disruption spreads up to half the minor radius.

From the soft X-ray emission (A having a dependence of $A \propto \sqrt{T_e}\exp(-Ec/T_e)$), the electron temperature oscillation $\tilde{T}_e$ can be deduced as

$$\tilde{T}_e/T_e = \left(\frac{1}{2} + \frac{E_c}{T_e}\right)^{-1} \tilde{A}/A \quad ,$$

where E_c (= 1.33 keV) is an energy constant associated with the X-ray detector foil. Here we assumed that the soft X-ray sawtooth oscillation comes only from the electron temperature oscillation. Using this dependence, the energy losses with internal disruption inside the q=1 magnetic surface is evaluated.

For circular discharges of B_T = 12 kG, q_a^* = 1.64, $\bar{n}_e$ = 4.7 × 10^{13} cm^{-3}, r_s/a = 0.49, the time-averaged loss power by internal disruption is 38% of the ohmic input inside the q = 1 magnetic surface. For a 1.5 elongated D-shaped discharge of B_T = 12 kG, q_a^* = 1.72, $\bar{n}_e$ = 4.2 × 10^{13} cm^{-3}, r_s/a = 0.45, the energy losses by internal disruption are 18% of the ohmic input inside the q=1 magnet surface. The difference in degree of internal disruption between circular and elongated discharges is due to the differences in $\tilde{A}/A$ shown in Fig. 13.

Another approach for seeing the effect of internal disruption on energy loss is the investigation of parameter dependence of internal disruption. The period of sawtooth oscillation t_s and the amplitude $\tilde{A}/A$ of soft X-ray emission are shown in Fig. 12 and 13 as a function of $\bar{n}_e/q_a^*$ and q_a^*, respectively.

Contradictory to the DIVA and TFR [14] results, Fig. 12 shows that t_s has no dependence on $\bar{n}_e/q_a^*$ for D-shaped (o) and circular (•) discharges. $\tilde{A}/A$ as a function of q_a^* shown in Fig. 13 is not simple; for a circular discharge, it remains almost constant in the area of 0.26-0.32 (with one exception attaining 0.4). For 1.5 elongated plasmas, it stays almost constant around 0.22 for $q_a^* \simeq 1.8 - 3.0$, and decreases down to around 0.14 at q_a^* = 1.5 - 1.7. As a result, there is a factor of two difference in $\tilde{A}/A$ for circular and elongated discharges at $q_a^* \lesssim 1.7$. This difference of MHD

property may be related to the increase of vertical elongation at the q=1 magnetic surface in D-shaped low-q plasmas. Again, $\tilde{A}/A$ shows no dependence such as $\sim q_a^{-3/2}$ observed in DIVA and TFR. Therefore, $\tilde{\tau}_{E_e}$ defined as Eq. (1) shows no dependence such as $\bar{n}_e\, q_a^{*1/2}$ nor $\bar{n}_e\, q_a^{*}$, so that internal disruption is not a major factor of energy confinement.

6. PLASMA-WALL INTERACTION

The severity of plasma-wall interaction for low-q discharge especially in large devices, was predicted in the DIVA experiments. In the low-q DIVA discharges, although no serious increase in radiative loss was found, a pulsive increment in the release of wall material was observed after each internal disruption. This was attributed to the increase in edge temperature caused by the pulsive heat released from the inside of the q = 1 magnetic surface close to the wall.

In terms of plasma-wall interaction, the low-q experiment in Doublet III is a good extension of DIVA for future large tokamak devices, since Doublet III has large ohmic input, up to 1.5 MW, compared with 0.2 MW in DIVA.

Figure 14 shows the ratio of radiation loss to ohmic input P_r/P_{OH} in the total plasma volume as a function of q_a^* for D-shaped discharges. The circles and triangles correspond to discharges with B_T = 12 kG and 24 kG respectively. For each q_a^*, the data point includes the operational electron density regime from lowest to highest. The figure shows that discharges of $q_a^* \lesssim 2$ typically have a P_r/P_{OH} of ~0.4, while those of $q_a^* > 4$ have a relatively high P_r/P_{OH} of ~0.5 - 0.7. Circular plasmas show the same behavior as D-shaped plasmas. This tendency indicates that the heat load on the limiters increases greatly during low-q operation.

A comparison of successive discharges with the same I_p and $\bar{n}_e$ for low-q (1.7) and relatively high-q (3.4) are shown in Fig. 15.

These discharges differ only in the toroidal field: B_T = 12 kG for q_a^* = 1.7, B_T = 24 kG for q_a^* = 3.4. The figure shows the comparison of I_p, $\bar{n}_e$, $\bar{n}_{e_{EDGE}}$ measured with a CO_2 laser interferometer looking 2 cm away from the inside backup limiter, spatially peaked heat flux into the inside back-up limiter measured with infra-red camera, VUV signal of NiXI 148Å, Ni XVIII 292 Å and OV 630 Å, and P_r, P_{OH} at the flattop.

Heat flux as measured by an infra-red camera looking at the inside backup limiter and a thermocouple probe installed at the top back-up limiter (not shown here), increases by a factor of 2 with low-q operation and corresponds well with the change in (P_{OH} - P_r).

Total radiation power measured with a bolometer array is mainly determined by the radiation at the outer half of the minor radius. From the VUV measurement of NiXI 148Å, NiXVIII 292Å (both Δn = 0 transitions), the amount of nickel is ~ 0.001% of $\bar{n}_e$ and the line radiation from the nickel is negligible. The radiation power due to the line radiation from the gaseous impurity is not clear, because our absolute intensity calibration at more than 300Å is incomplete, where most of the strong resonance lines of oxygen occur. However, from the OV 630Å by VUV observation, and CIII 4647Å, OI 7773Å and H_α by filtered photo-diode observation, the increase in radiation from the periphery in high-q discharge is considered to be attributed to increased recycling of gaseous impurities.

The most significant change is in the formation of high edge density at the inside backup limiter. The phenomenon was originally studied by D. Baker, et al., [15], and was found that the high edge density layer appears when $\bar{n}_e/(P_{OH} - P_r)$ exceeds a critical value. The Ni XI radiation intensity, which is proportional to nickel influx, does not change although the heat flux to the limiter increases by a factor of 2 with low-q operation. One possible answer is in an experiment using Ne injection during the discharge. The Ne injection experiment was originally planned to study the radiative cooling of the plasma periphery with low-Z impurity in order to reduce the production of limiter material impurity [16]. In terms of the stated purpose, our trial failed, i.e., an increase of Ni XI was observed with Ne injection for both low-q and high-q discharge although the radiation loss increased with injection. This implies that under clean surface conditions, contamination of the plasma with low-Z impurity is more effective in increasing incident ion flux to the limiter rather than decreasing the edge temperature in the ion-sputtering process [17]. A similar phenomenon was observed with Ne injection into the JFT-2 plasma [18] with a molybdenum limiter. Applying this observation to both high-q and low-q discharges, the increase in recycling flux of low-Z impurity ions during high-q discharge may compensate for the reduction in edge temperature due to larger radiation.

The line-integrated Ni XVIII intensity during low-q discharge is a factor of 2 higher than that during high-q discharge. Using an impurity transport code [18], the difference in line-integrated emissivity is

explained by that of electron temperature with the same amount of nickel in the discharge; $T_e(0)$ = 450 eV for 12 kG and 810 eV for 24 kG. Here we employed neoclassical transport superimposed by an anomalous diffusion of 5 $\times 10^3$ cm^2/sec, which gives the best agreement with observation of the intensity ratio of nickel lines of several charged states.

In conclusion, no serious increase of metallic impurity contamination was observed during low-q discharge, although the heat flux increased by a factor of 2. In future tokamak devices with higher heating power, the increase in heat flux will become a serious problem resulting in a melting of the limiter. An improvement in the limiter, for example, one which accepts heat over a larger area, may be necessary.

7. CONCLUSIONS

An optimum low-q operation regime, which can be applied to future D-shaped cross section high-β tokamaks without a conducting shell, was explored in Doublet III. The stable discharge with $q_a^{\psi} < 2$ was not realized in this experiment. However, a low-q regime, which is expected to improve the high-β capability of tokamaks, was found in D-shaped plasmas. The low-q discharges with D-shaped plasmas also show excellent plasma performance. The results are summarized as follows:

1. q_a^* as low as 1.5 and 1.7 was realized for 1.5 elongated D-shaped and circular cross section plasmas. The actual MHD q_a (q_a^{ψ}) was a factor of 1.5 and 1.2 larger than q_a^* for D-shaped and circular cross sections, respectively. Because of the strong toroidal and shaping field effect on the rotational transform at the outer plasma edge associated with D-shape formation, the q^{ψ}-value sharply increase at the plasma outer edge, thus D-shaped plasmas show very high plasma current operational capabilities. With this low-q discharge, the q^{ψ} value at the energy confinement region is small, i.e., $q^{\psi} < 1.5$ at $r/a < 0.86 - 0.9$ for $q_a^{\psi} = 2.9 - 2.5$.

2. Important operation conditions to achieve low-q discharge were 1) clean wall and limiter surface conditions, 2) precise plasma position conditioning, 3) slow ramping of plasma current,

and 4) precise control of gas puff throughput during the current ramping phase. Most of these operations are directly related to the control of metallic impurities influx.

3. For D-shaped plasmas, the reproducible stable operation region can be simplified as between $I_p/\bar{n}_e$ = 1.1 and 2.2 MA/10^{14} cm^{-3}, and q_a^{ψ} less than 2.4 (q_a^* ~ 1.5). The probability of disruption was 12% for the discharges aiming the $\bar{n}_e$ - I_p at the flattop within this stable region. In the future, the probability of disruption is expected to be reduced significantly with careful operation, because the disruptions in the present experiment occurred only near the boundary of the stable region, or outside due to the change of wall surface condition during a repeated operation.

4. Low-q discharges, especially for D-shaped plasmas, show excellent plasma performance: 1) high density operational capabilities of $\bar{n}_e$ R/B_T reaching 7.8; 2) good energy confinement resulting in volume average β reaching 1% with ohmic heating only.

5. Energy confinement time in this low-q regime is fairly applicable to recent tokamak reactor design. Gross energy confinement time τ_E scales as τ_E[sec] = 0.06 $\bar{n}_e$ [× 10^{14} cm^{-3}] $q_a^{*0.84}$ in this low-q regime, where neoclassical heat loss of ions is not important. This scaling shows an identical τ_E as the INTOR scaling (τ_E[sec] = 0.5 $\bar{n}_e$ [× 10^{14} cm^{-3}] a[m]^2) at q_a^* = 1.8. Internal disruption

seems to play an important but not dominant role in electron energy loss. Some difference in sawtooth activity between D-shaped and circular cross section plasmas was found at lowest q, where the vertical elongation of the q=1 magnetic surface is strong.

6. Plasma-wall interaction becomes a serious problem in low-q operation. This is caused by the reduction of radiative loss at the plasma periphery, which is attributed to the reduction of particle recycling at the periphery in low-q operation.

ACKNOWLEDGEMENT

The continuing support of Drs. S. Mori, Y. Iso, K. Tomabechi, Y. Obata, M. Yoshikawa of JAERI, and Dr. T. Ohkawa of GAC is gratefully acknowledged. This experiment was carried out with the fine support of the Doublet III diagnostics group under Dr. R. Fisher and the machine operation group under Dr. R. Callis.

This work was authorized by a cooperative agreement between the Japan Atomic Energy Research Institute and the United States Department of Energy under DOE Contract No. DE-AT03-80SF11512.

seems to play an important but not dominant role in electron energy loss. Some difference in sawtooth activity between D-shaped and circular cross section plasmas was found at lowest q, where the vertical elongation of the q=1 magnetic surface is strong.

6. Plasma-wall interaction becomes a serious problem in low-q operation. This is caused by the reduction of radiative loss at the plasma periphery, which is attributed to the reduction of particle recycling at the periphery in low-q operation.

ACKNOWLEDGEMENT

The continuing support of Drs. S. Mori, Y. Iso, K. Tomabechi, Y. Obata, M. Yoshikawa of JAERI, and Dr. T. Ohkawa of GAC is gratefully acknowledged. This experiment was carried out with the fine support of the Doublet III diagnostics group under Dr. R. Fisher and the machine operation group under Dr. R. Callis.

This work was authorized by a cooperative agreement between the Japan Atomic Energy Research Institute and the United States Department of Energy under DOE Contract No. DE-AT03-80SF11512.

REFERENCES

[1] SWAIN, D. W., MURAKAMI, M., BATES, S. C., DUNLAP, J. L., EDMONDS, P. H., et al., Bulletin of the Americal Physical Society, 25 (1980) 875.

[2] MURAKAMI, M., SWAIN, P. W., BATES, S. C., BUSH, C. E., CHARLTON, L. A., et al., in Plasma Physics and Controlled Nuclear Fusion Research (Proc. 8th Int. Conf. Brussels, 1980) IAEA-CN-38/N-1.
SUZUKI, N., et al., ibid, IAEA-CN-38/t-2-3.

[3] ELLIS, J. J., McGUIRE, K. M., PEACOCK, R., ROBINSON, D. C., STARES, I., in Plasma Physics and Controlled Nuclear Fusion Research (Proc. 8th Int. Conf. Brussels, 1980) IAEA-CN-38/X4-4.

[4] LEONOV, V. M., MEREZHKIN, V. G., MUKHOVATOV, V. S., SANNIKOV, V. V., TILININ, G. N., Ibid., IAEA-CN-38/N-2.

[5] BERLIZOV, A. B., BUGARAYA, V. I., BUZANKIN, V. V., VASIN, N. L., VERTIPOROCH, A. N., et al., Ibid., IAEA-CN-38/A-2.

[6] OVERSKEI, D. O., private communication.

[7] DIVA Group, Nucl. Fusion 20 (1980) 271. YAMAMOTO, S., SENGOKU, S., MATSUDA, T., MATSUMOTO, H., OHASA, K., et al., Jap. J. Ap. Phys. 19 (1980) 413.

[8] CALLIS, R. W., Doublet III Baseline Design Description, GA-A13996.

[9] STAMBAUGH, R., ADCOCK, S., CALLIS, R., DeGRASSIE, J., LUXON, J., et al., Plasma Equilibrium Control in Doublet III, GA-A16049.

[10] McCLAIN, R. W., BROWN, B. B., GAQ, A Computer Program to Find and Analyze Axisymmetric MHD Plasma Equilibria, GA-A14490 (1977).

[11] TOI, K., ITOH, S., KADOTA, K., KAWAHATA, K., NODA, N., et al., Nucl. Fusion 19 (1979). 1643.

[12] NAGAMI, M., YOKOMIZO, H., SHIMADA, M., YOSHIDA, H., IOKI, K., et al., Energy Confinement of Ohmically Heated D-Shaped Plasmas in Doublet III, JAERI-M 9509 (1981).

[13] KITSUNEZAKI, A., FUJISAWA, N., IOKI, K., KONOSHIMA, S., NAGAMI, M., et al., in Plasma Physics and Controlled Nuclear Fusion Research (Proc. 8th Int. Conf. Brussels, 1980) IAEA-CN-38/N-3.

[14] TFR Group, in Plasma Physics and Controlled Nuclear Fusion Research (Proc. 6th Int. Conf. Berchtesgarden, 1976), Vol. 1, IAEA, Vienna (1977) 279.

[15] BAKER, D. R., NAGAMI, M., SNIDER, R. T., Observation of Cold, High-Density Plasma Near the Doublet III Limiter, GA-A16337 (1981).

[16] NAGAMI, M., Radiative Cooling in the Outer Edge of a Tokamak Plasma by Low-Z Impurities, JAERI-M 7432 (1977).
SHIMOMURA, Y., Nucl. Fusion 17 (1977) 626.

[17] OHASA, K., MAEDA, H., YOMAMOTO, S., NAGAMI, M., OHTSUKA, H., Nucl. Fusion 18 (1978) 872.

[18] SUZUKI, N., FUJISAWA, N., KONOSHIMA, S., MAENO, M., SHIMADA, M., et al., in Controlled Fusion and Plasma Physics (9th Europ. Conf., Oxford, 1979).

[19] WONG, S. K., A Trace Impurity Transport Code, GTA-A15323 (1979).

FIGURE CAPTIONS

Fig. 1 Cross sectional view of Doublet III device.

Fig. 2 Equilibrium and waveforms of plasma current and loop voltage for typical lowest q discharges with D-shaped and circular cross section. Plasma position control is terminated at around t = 890 msec.

Fig. 3 Comparison of q^{ψ} profile for discharges with D-shaped and circular cross sections. q^{ψ} increases very rapidly near the plasma surface for D-shaped plasmas due to strong toroidal and shaping field effects; $q_a{}^{\psi}/q_a{}^{*} = 1.52$ for the D-shaped plasma, $q_a{}^{\psi}/q_a{}^{*} = 1.20$ for the circular plasmas.

Fig. 4(a) Observation of the magnetic surface of sawtooth inversion with vertical and tangential soft X-ray diode arrays for discharges with $q_a{}^{*}$ = 1.5, 2.1, 3.1.

Fig. 4(b) Vertical elongation of the magnetic surface of sawtooth inversion (horizontal radius of r_s) measured with soft X-ray diode arrays and that of the outermost magnetic surface calculated with MHD equilibrium code. For a constant shape control of the magnetic flux surface at the shaping coils, elongation of the magnetic surface of sawtooth inversion increases with the decrease of $q_a{}^{*}$. At the same time, elongation of the outermost magnetic surface increases slightly. For simplicity, we will refer to $K_a = 1.47$ for D-shaped plasmas with arbitrary $q_a{}^{*}$ from Fig. 4. The toroidal and shaping field effects on $q_a{}^{\psi}$ stays almost constant with $q_a{}^{*}$.

Fig. 4(c) Horizontal radius of the magnetic surface of sawtooth inversion for D-shaped and circular cross section plasmas.

Fig. 5 Comparison of stable operational region in $\bar{n}_e$-I_p space for D-shaped and circular cross section plasmas at the plasma current flattop. D-shaped plasmas with 1.5 elongation have a factor of two higher plasma current operation capability than circular plasmas.

Fig. 6 Stability of discharges as a function of gas puff throughput during plasma current ramping. Adjusting the intensity of gas puff throughput is the essential feature in order to achieve low-q discharges.

Fig. 7 Probability of disruption as a function of programmed plasma current at the flattop. At $I_p < 900$ kA, total probability of disruptions was 12%: total 165 shots, stable 145 shots (88%), disruption 20 shots (12%) (during flattop 6 shots, during current ramp 14 shots).

Fig. 8 Location of disruption in $\bar{n}_e$-I_p space for all the disruptive shots (20 shots) with programmed I_p at flattop of < 900 kA. Disruptions occur only outside or near-inside the boundary of the stable region during repeated operations. This indicates the possibility of great reduction in the disruption probability with more careful operation.

Fig. 9 Improvement of stable operational regime with the changing of the wall conditioning and selection of the primary limiter material. In the present low-q experiment, $\bar{n}_e R/B_T$ reaches 7.8 for D-shaped plasmas with ohmic heating only.

Fig. 10 Electron temperature profiles measured with scanning soft X-ray spectrometer for D-shaped discharges with $q_a^* = 1.5$ and 2.9. The volume average β reaches 1.0% with ohmic heating only.

Fig. 11 Least square fitting of the data shows that gross electron energy confinement time scales as τ_E [msec] = 30 $\bar{n}_e$ [$\times 10^{14}$ cm^{-3}] $q_a^{*0.84}$.

Fig. 12 The sawtooth period of soft X-ray t_s shows no dependence on $\bar{n}_e/q_a^*$.

Fig. 13 Amplitude of sawtooth show no clear dependence on q_a^*. The amplitude for D-shaped plasmas is a factor of two lower than that for circular plasmas at $q_a^* \lesssim 1.7$.

Fig. 14 The fraction of radiative loss power to the ohmic input increases with the increase of q_a^*.

Fig. 15 Comparison of plasma-wall interaction for discharges with the same plasma current of 750 kA and different B_T: B_T = 12 kG, $q_a^* = 1.7$ and B_T = 24 kG, $q_a^* = 3.4$. Low-q discharge reduces the radiative loss power, and results in an increase of heat flux to the limiter. No increase of influx and accumulation of metallic impurity was found.

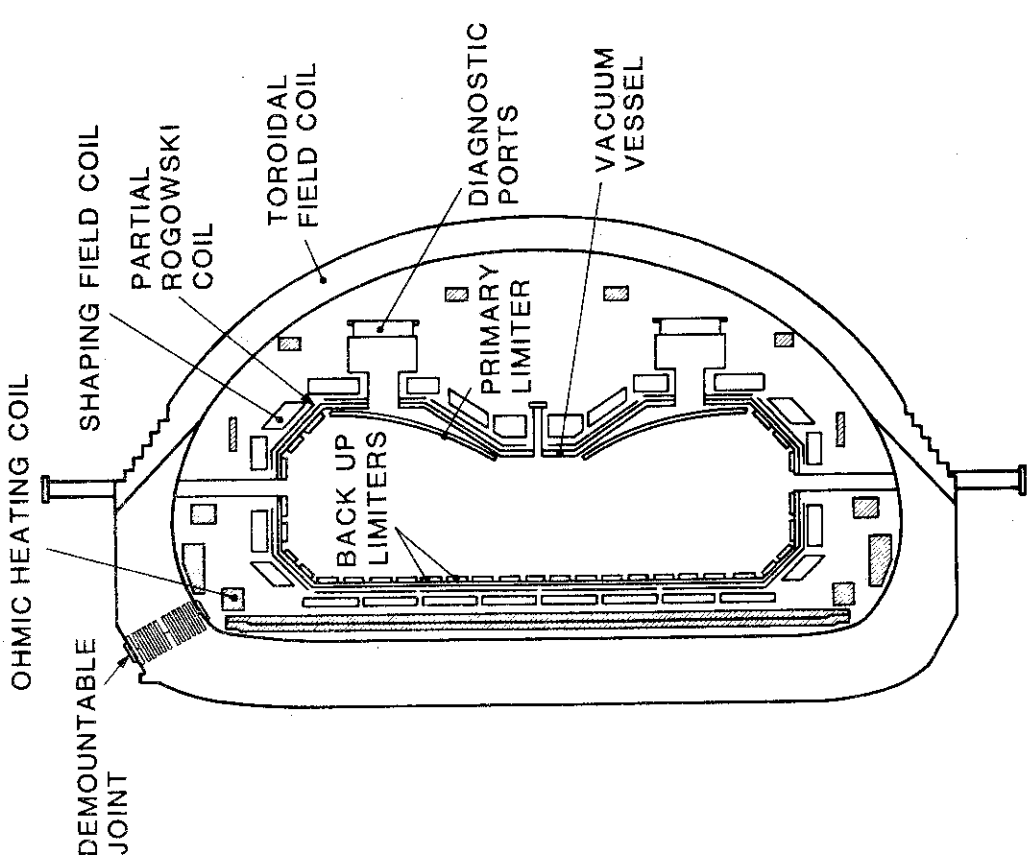
OHMIC HEATING COIL
SHAPING FIELD COIL
PARTIAL ROGOWSKI COIL
TOROIDAL FIELD COIL
DIAGNOSTIC PORTS
VACUUM VESSEL
PRIMARY LIMITER
BACK UP LIMITERS
DEMOUNTABLE JOINT

Fig. 1

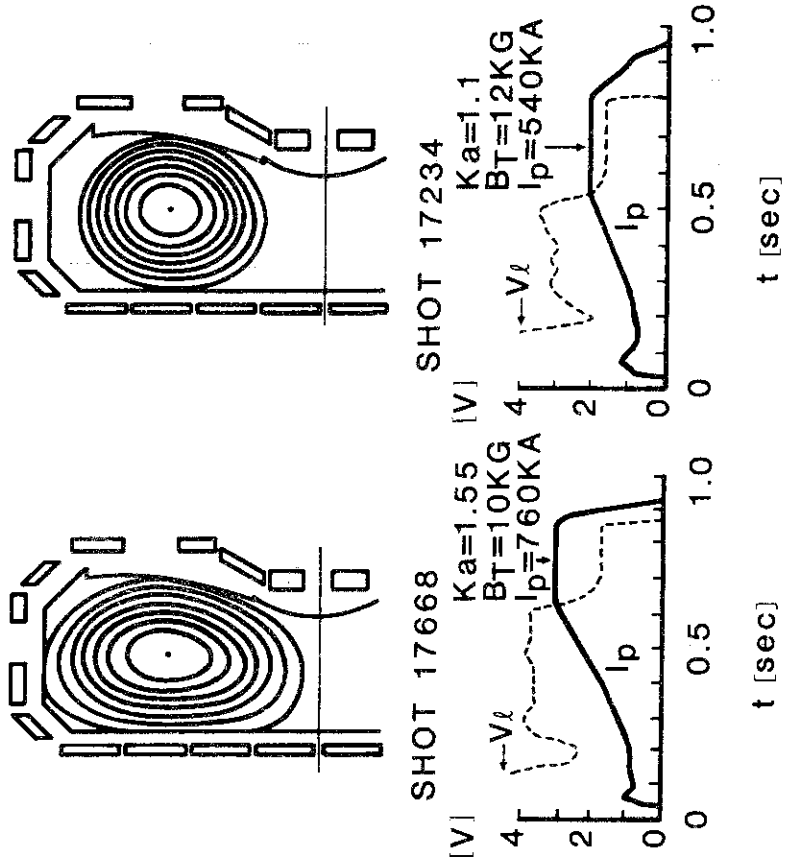
SHOT 17668
Ka=1.55
BT=10KG
Ip=760KA
SHOT 17234
Ka=1.1
BT=12KG
Ip=540KA
Vℓ
Ip
[V]
t [sec]

Fig. 2

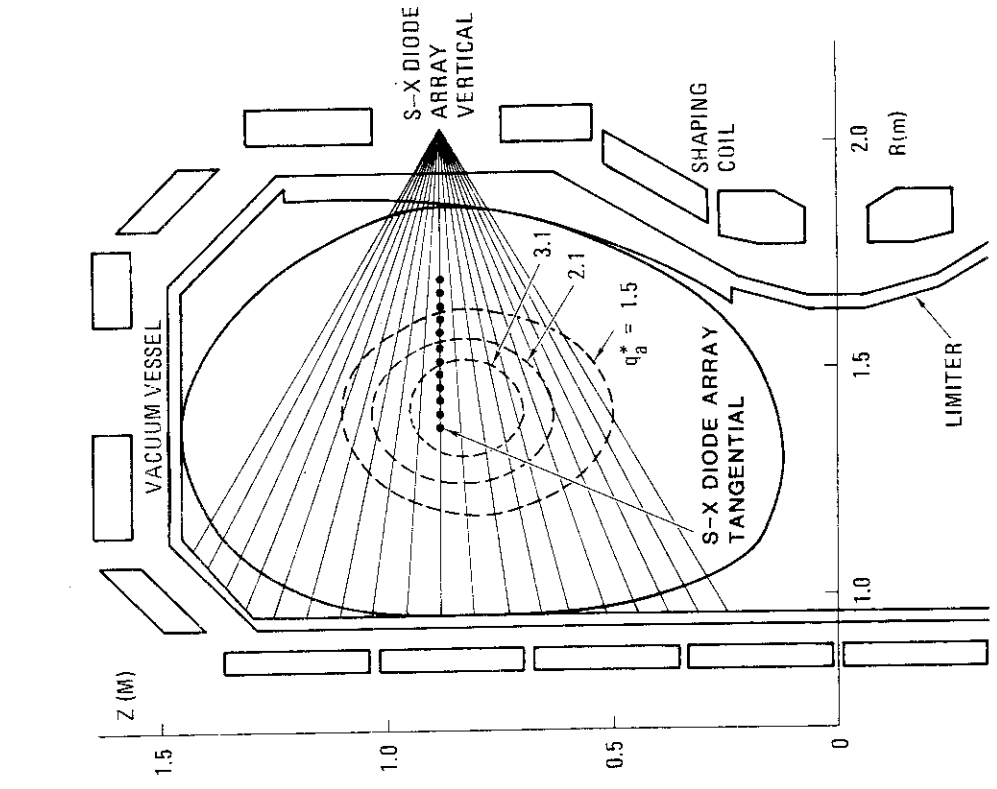
S-X DIODE ARRAY VERTICAL
SHAPING COIL
VACUUM VESSEL
3.1
2.1
$q_a^* = 1.5$
S-X DIODE ARRAY TANGENTIAL
LIMITER
Z (M)
R(m)
1.5
1.0
0.5
0
2.0

Fig. 4(a)

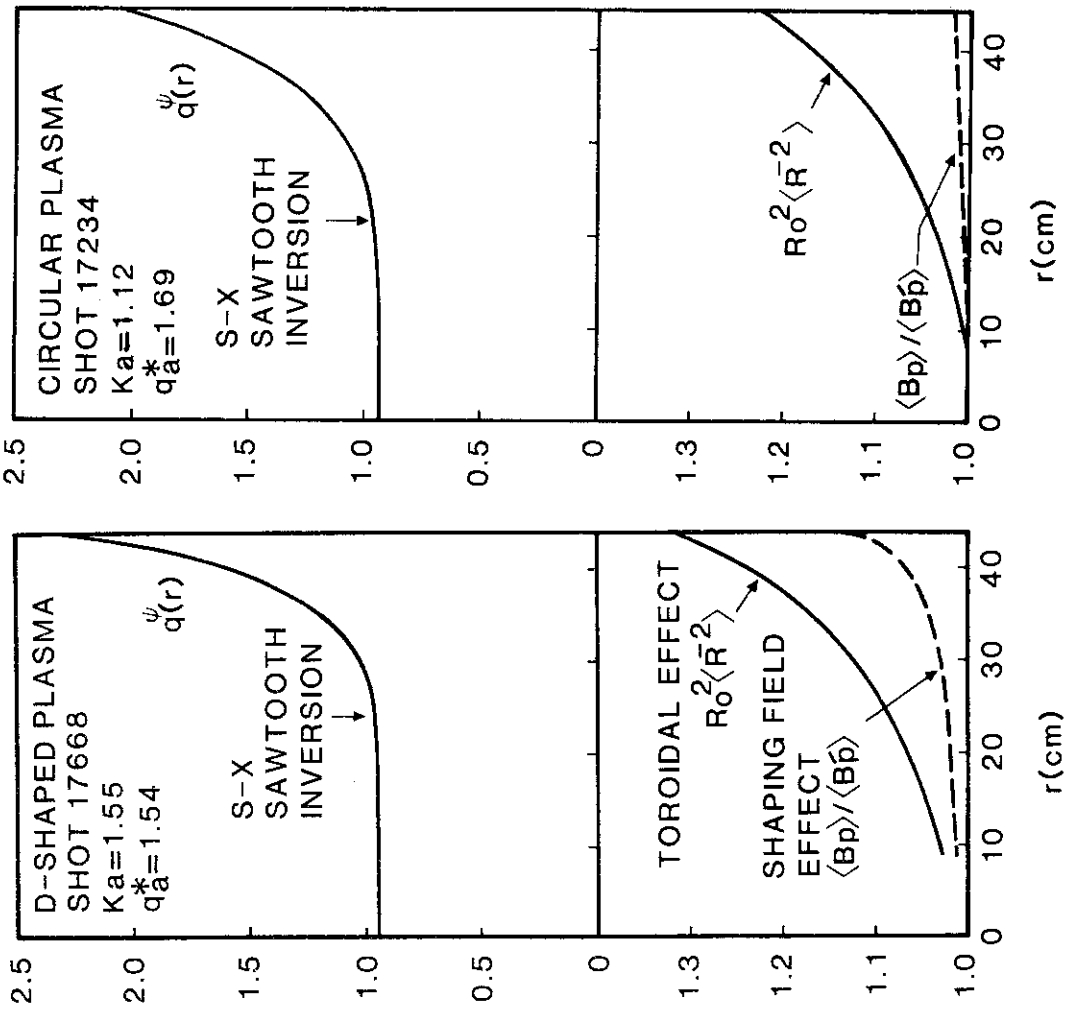
CIRCULAR PLASMA
SHOT 17234
Ka=1.12
q_a^*=1.69
ψq(r)
S-X SAWTOOTH INVERSION
$R_o^2\langle R^{-2}\rangle$
$\langle Bp\rangle/\langle B\bar{p}\rangle$
D-SHAPED PLASMA
SHOT 17668
Ka=1.55
q_a^*=1.54
TOROIDAL EFFECT
SHAPING FIELD EFFECT
r(cm)

Fig. 3

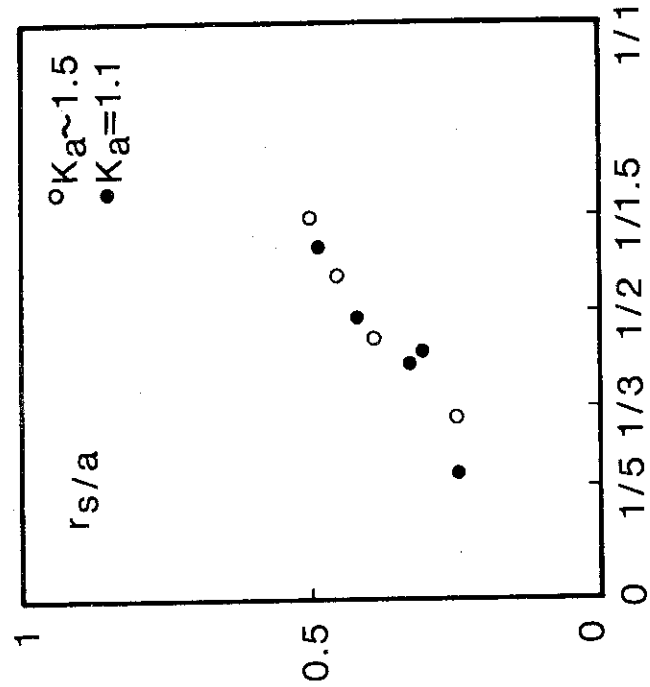
°Ka~1.5
•Ka=1.1
r_s/a
1
0.5
0
0 1/5 1/3 1/2 1/1.5 1/1
$1/q_a^*$

Fig. 4(c)

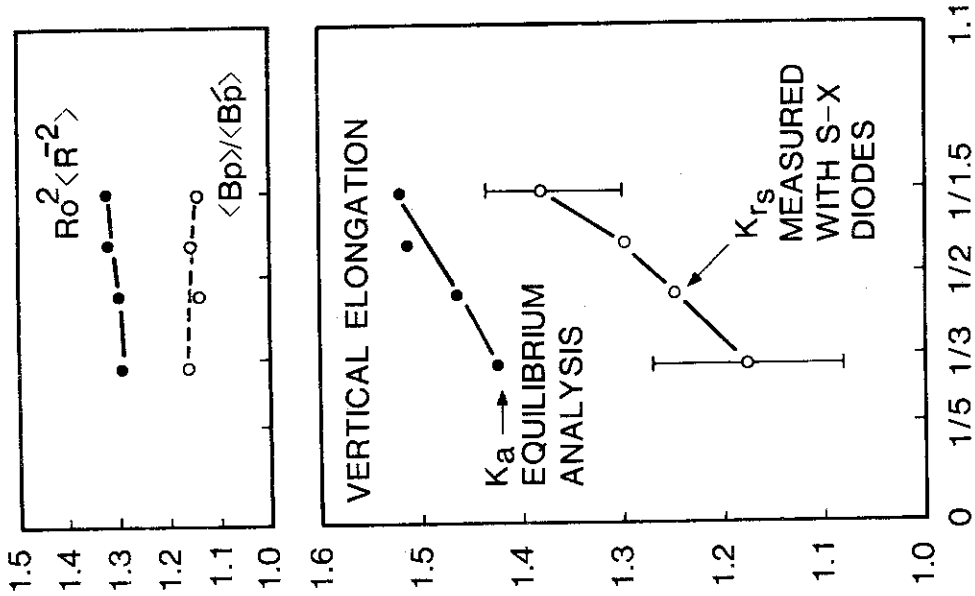
$R_o^2\langle R^{-2}\rangle$
$\langle Bp\rangle/\langle B\bar{p}\rangle$
1.5
1.4
1.3
1.2
1.1
1.0
VERTICAL ELONGATION
K_a → EQUILIBRIUM ANALYSIS
K_{r_s} MEASURED WITH S-X DIODES
1.6
1.5
1.4
1.3
1.2
1.1
1.0
0 1/5 1/3 1/2 1/1.5 1.1
$1/q_a^*$

Fig. 4(b)

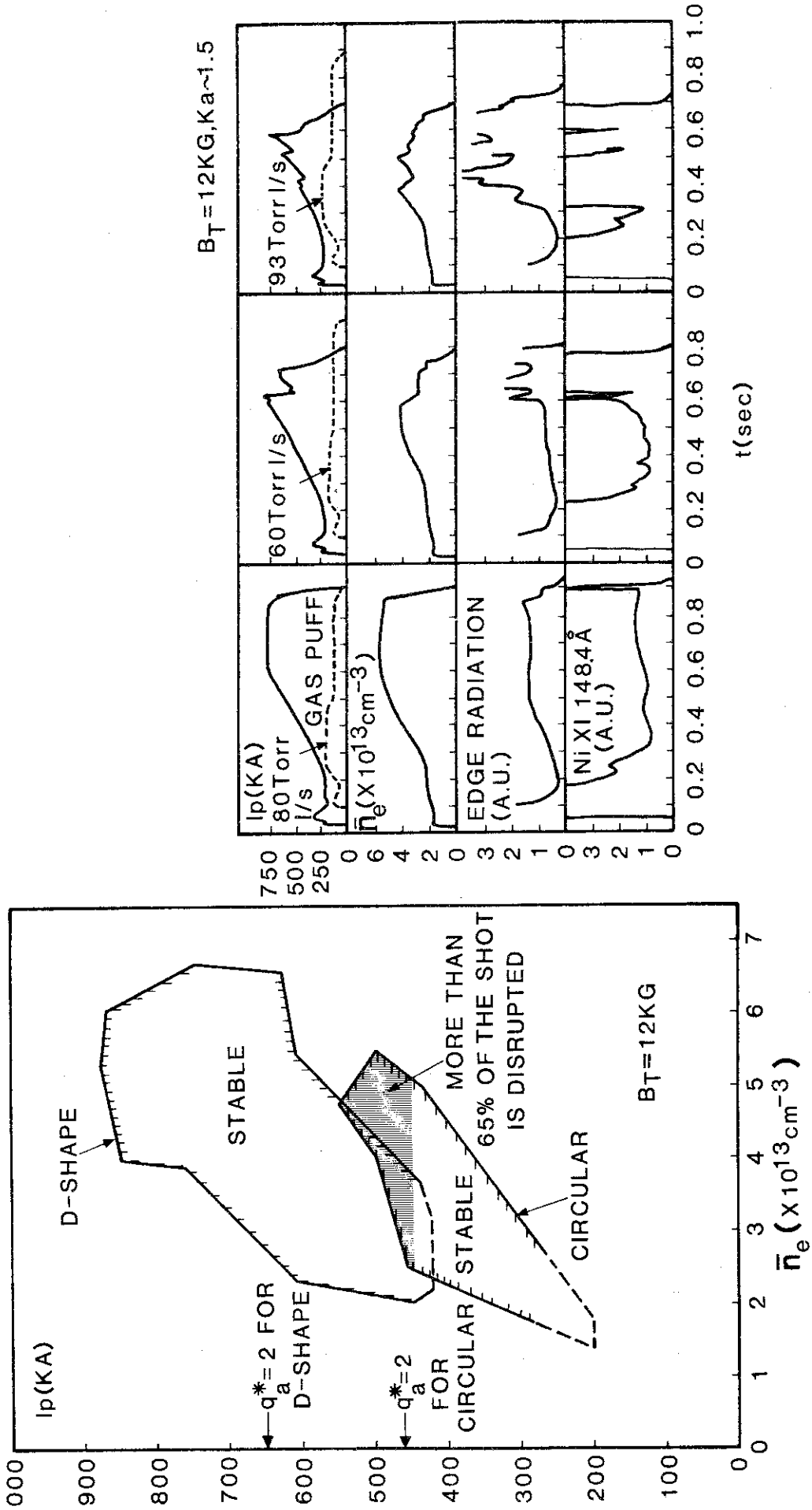
Ip(KA)
D-SHAPE
STABLE
q_a^*= 2 FOR D-SHAPE
q_a^*=2 FOR CIRCULAR
STABLE
MORE THAN 65% OF THE SHOT IS DISRUPTED
CIRCULAR
B_T=12KG
$\bar{n}_e$ ($X10^{13}cm^{-3}$)
B_T=12KG,Ka~1.5
Ip(KA)
80Torr l/s
GAS PUFF
60Torr l/s
93Torr l/s
$\bar{n}_e$($X10^{13}cm^{-3}$)
EDGE RADIATION (A.U.)
Ni XI 1484Å (A.U.)
t(sec)

Fig. 5

Fig. 6

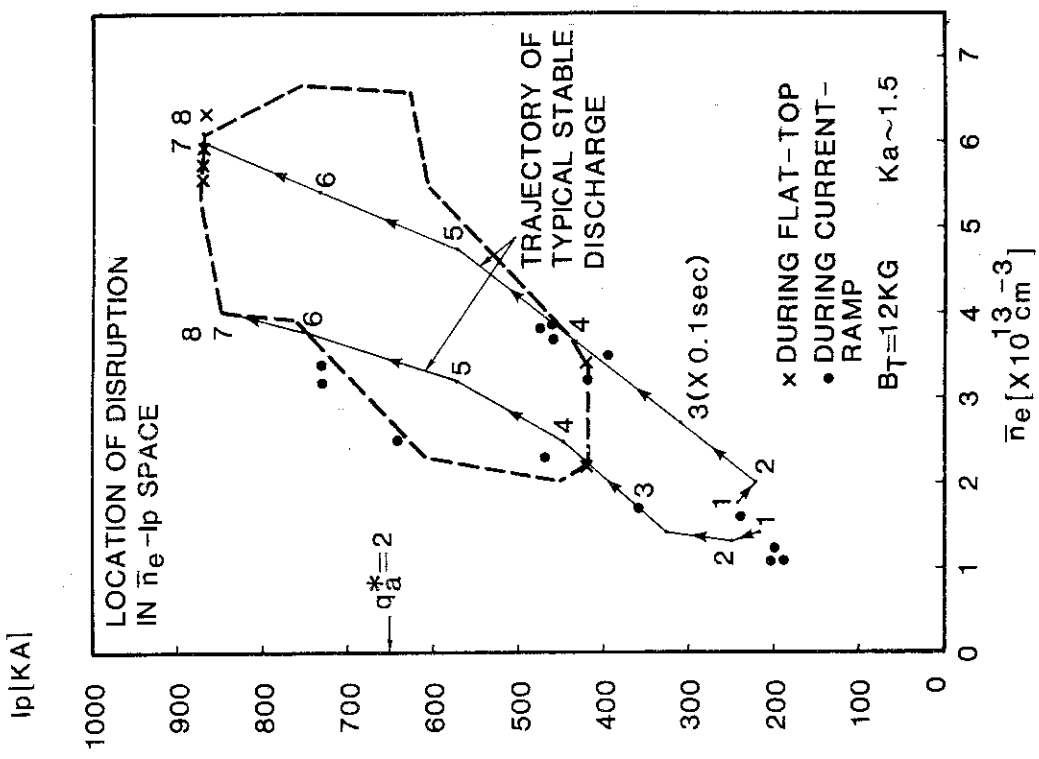
Ip[KA]
LOCATION OF DISRUPTION
IN $\bar{n}_e$-Ip SPACE
TRAJECTORY OF TYPICAL STABLE DISCHARGE
3(X 0.1sec)
$q_a^*=2$
× DURING FLAT-TOP
• DURING CURRENT-RAMP
B_T=12KG Ka~1.5
$\bar{n}_e$[X10^{13}cm^{-3}]

Fig. 8

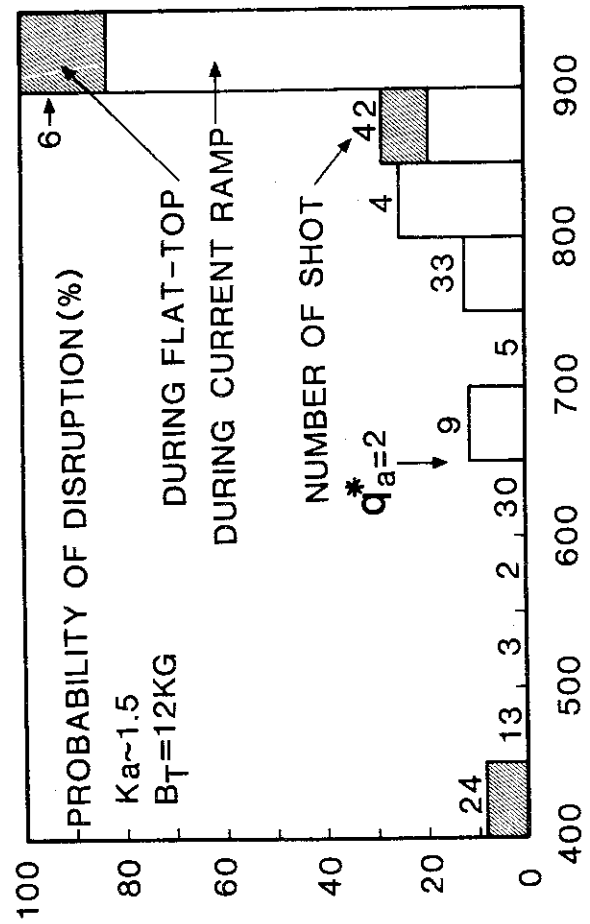
PROBABILITY OF DISRUPTION (%)
Ka~1.5
B_T=12KG
DURING FLAT-TOP
DURING CURRENT RAMP
NUMBER OF SHOT
$q_{a=2}^*$
PROGRAMMED Ip(KA)

Fig. 7

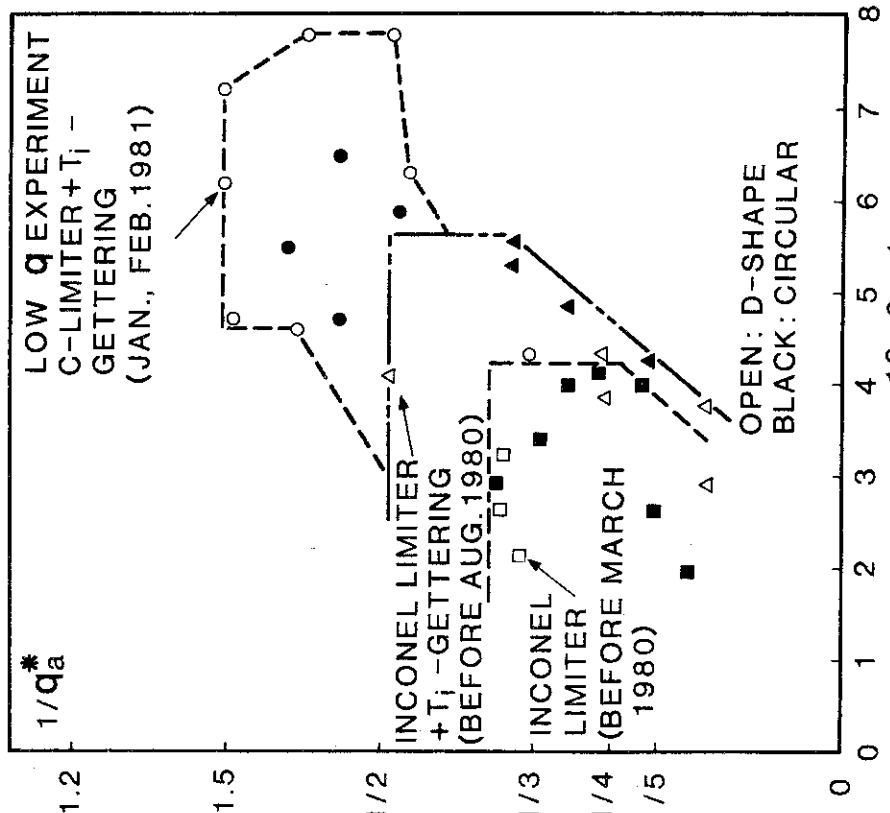
LOW q EXPERIMENT
C-LIMITER+Ti-GETTERING
(JAN., FEB.1981)
INCONEL LIMITER +Ti-GETTERING (BEFORE AUG.1980)
INCONEL LIMITER (BEFORE MARCH 1980)
OPEN: D-SHAPE
BLACK: CIRCULAR
1/q*a
1/1.2
1/1.5
1/2
1/3
1/4
1/5
0
1
2
3
4
5
6
7
8
n̄e R/BT (X10^19 m^-2 T^-1)

Fig. 9

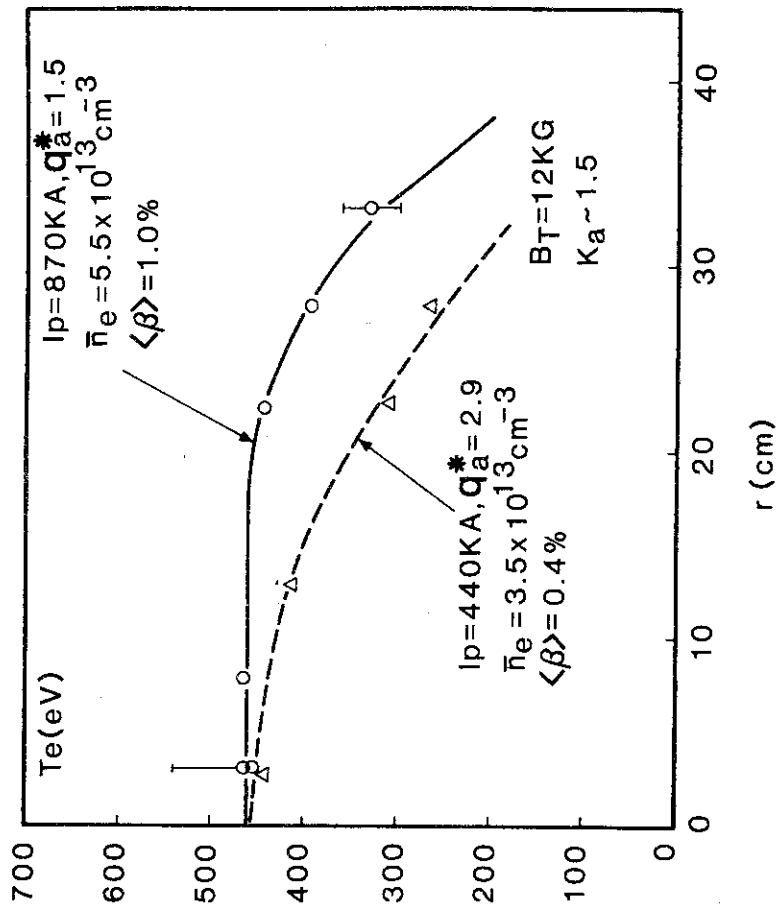
Te(eV)
Ip=870KA, q*a=1.5
n̄e=5.5x10^13 cm^-3
⟨β⟩=1.0%
Ip=440KA, q*a=2.9
n̄e=3.5x10^13 cm^-3
⟨β⟩=0.4%
BT=12KG
Ka~1.5
700
600
500
400
300
200
100
0
0
10
20
30
40
r (cm)

Fig. 10

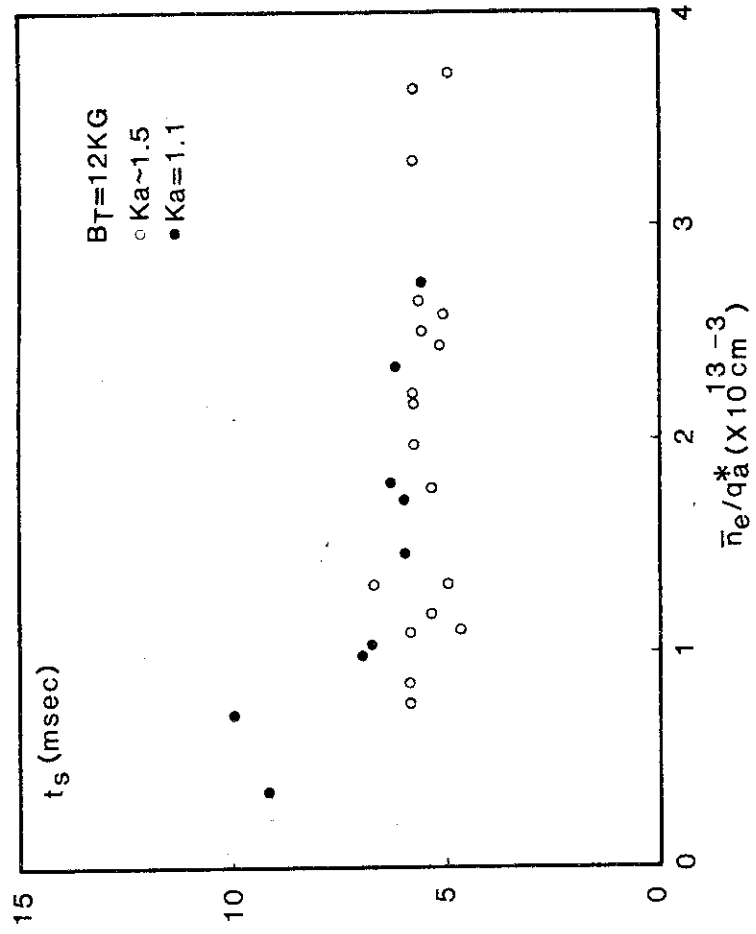
B_T=12KG
○ Ka~1.5
● Ka=1.1
t_s (msec)
$\bar{n}_e/q_a^*$ (X10^{13}cm^{-3})
0
5
10
15
0
1
2
3
4

Fig. 12

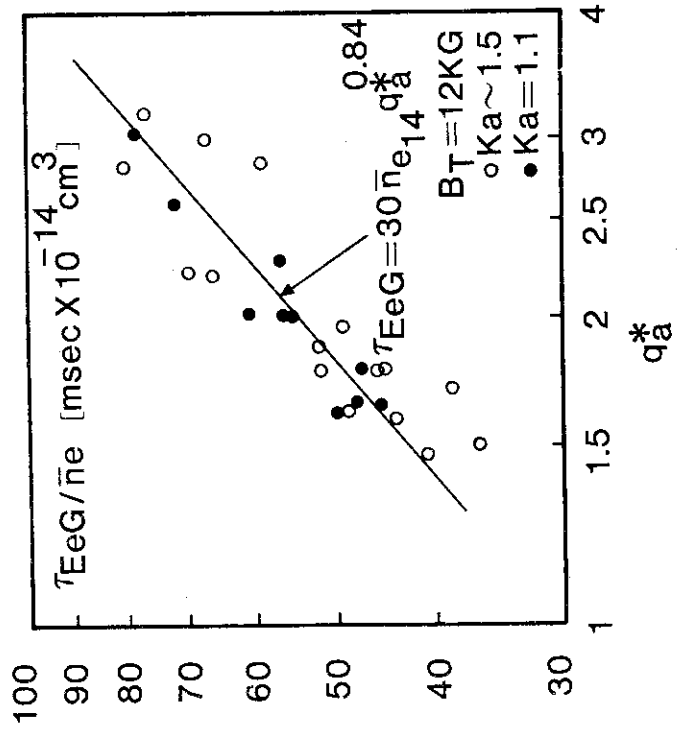
$\tau_{EeG}/\bar{n}e$ [msec X10^{-14}cm^3]
$\tau_{EeG}=30\bar{n}_{e14}^{0.84}q_a^*$
B_T=12KG
○ Ka~1.5
● Ka=1.1
q_a^*
30
40
50
60
70
80
90
100
1
1.5
2
2.5
3
4

Fig. 11

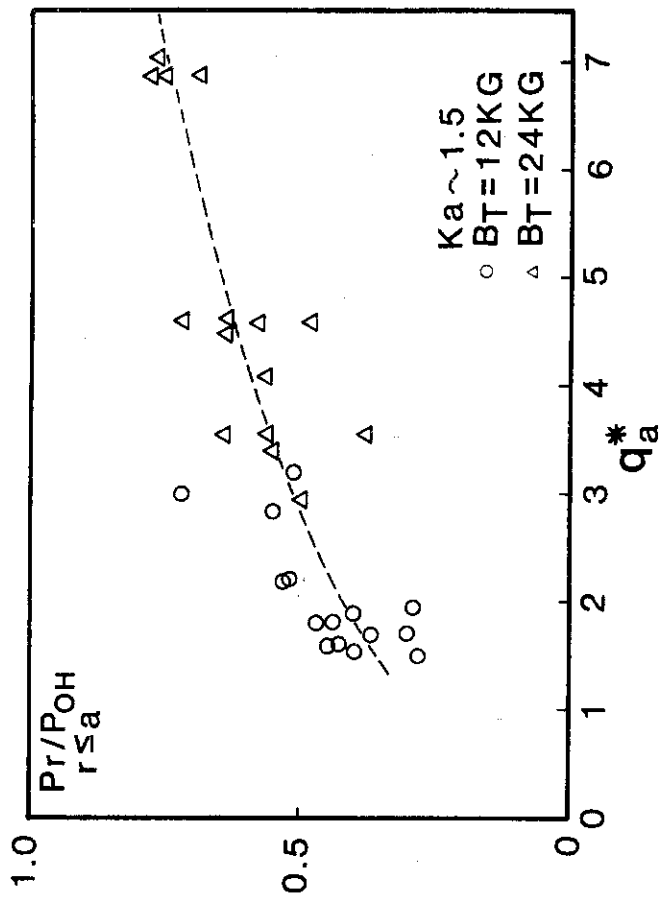

Fig. 14

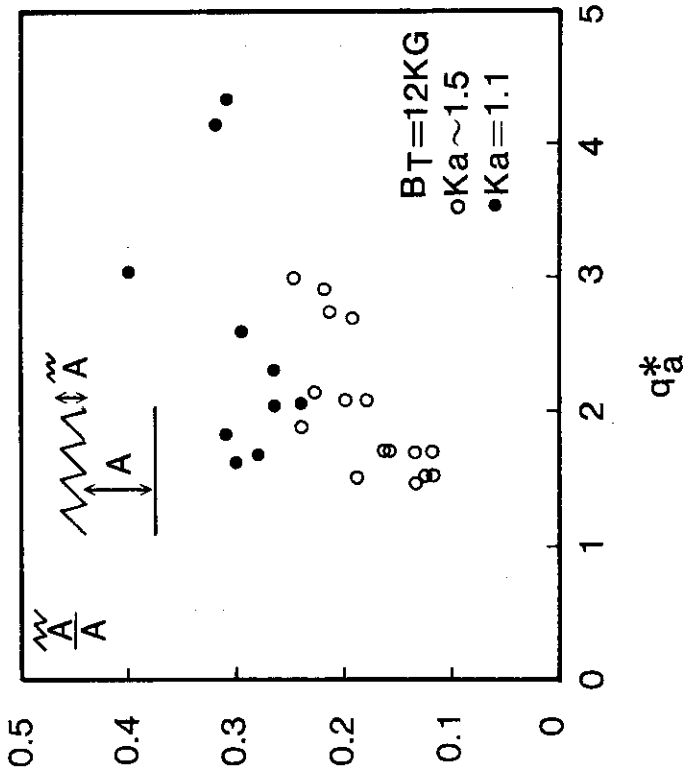

Fig. 13

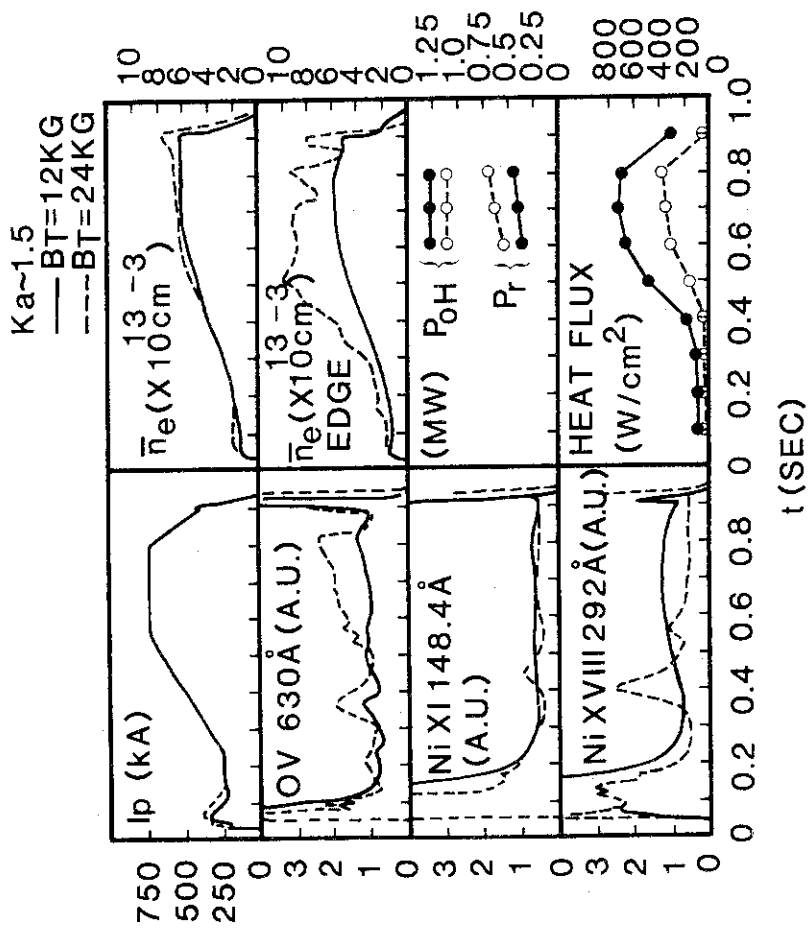
Ka~1.5
BT=12KG
BT=24KG
Ip (kA)
$\bar{n}_e$(X10^{13}cm^{-3})
$\bar{n}_e$(X10^{13}cm^{-3}) EDGE
(MW) P_{OH}
P_r
HEAT FLUX (W/cm^2)
OV 630Å (A.U.)
Ni XI 148.4Å (A.U.)
Ni XVIII 292Å(A.U.)
t (SEC)

Fig. 15